PHYSICAL REVIEW D **87,** 064033 (2013)

Outlook for detection of GW inspirals by GRB-triggered searches in the advanced detector era

Alexander Dietz
Department of Physics and Astronomy, University of Mississippi, Oxford, Mississippi 38677, USA

Nickolas Fotopoulos and Leo Singer
LIGO Laboratory, California Institute of Technology, Pasadena, California 91125, USA

Curt Cutler
Jet Propulsion Laboratory, California Institute of Technology, Pasadena, California 91109, USA
(Received 16 October 2012; published 22 March 2013)

Short, hard gamma-ray bursts (GRBs) are believed to originate from the coalescence of two neutron stars (NSs) or a NS and a black hole (BH). If this scenario is correct, then short GRBs will be accompanied by the emission of strong gravitational waves (GWs), detectable by GW observatories such as LIGO, Virgo, KAGRA, and LIGO-India. As compared with blind, all-sky, all-time GW searches, externally triggered searches for GW counterparts to short GRBs have the advantages of both significantly reduced detection threshold due to known time and sky location and enhanced GW amplitude because of face-on orientation. Based on the distribution of signal-to-noise ratios in candidate compact binary coalescence events in the most recent joint LIGO-Virgo data, our analytic estimates, and our Monte Carlo simulations, we find an effective sensitive volume for GRB-triggered searches that is ≈ 2 times greater than for an all-sky, all-time search. For NS-NS systems, a jet angle $\theta_j = 20°$, a gamma-ray satellite field of view of 10% of the sky, and priors with generally precessing spin, this doubles the number of NS-NS short-GRB and NS-BH short-GRB associations, to ~3–4% of all detections of NS-NSs and NS-BHs. We also investigate the power of tests for statistical excesses in lists of subthreshold events, and show that these are unlikely to reveal a subthreshold population until finding GW associations to short GRBs is already routine. Finally, we provide useful formulas for calculating the prior distribution of GW amplitudes from a compact binary coalescence, for a given GW detector network and given sky location.

DOI: 10.1103/PhysRevD.87.064033 PACS numbers: 04.30.Db

I. INTRODUCTION

We currently sit between the first and second generations of kilometer-scale, ground-based interferometric gravitational wave (GW) detectors. The first direct detection of GWs will very likely occur before the end of the decade.

The first detected signals will probably be from mergers of neutron star-neutron star (NS-NS), neutron star-black hole (NS-BH), and black hole-black hole (BH-BH) binaries, collectively referred to as compact binary coalescences, or CBCs. NS-NS and NS-BH coalescences are also likely progenitors for most short gamma-ray bursts (GRBs) [1,2]. It is therefore natural to use detections of short GRBs to trigger searches for GW signatures of CBCs that occur at the same instant (to within a few seconds) and the same sky location (within the error bars). Such GRB-triggered searches for GWs from CBCs are already being carried out [3–5].

In this paper, we address several questions regarding GRB-triggered CBC searches. We begin by reviewing recent results from such searches in Sec. I B and consider what GW and GRB detectors will be available in the advanced detector era in Sec. II. In Sec. III, we discuss the two most important factors in the detectability of GW counterparts of GRBs: namely, enhanced GW amplitude due to preferentially low binary inclination, and the reduced GW detection threshold resulting from knowledge of the GRB's time. Our primary results appear in Sec. IV, in which we estimate the rate of coincident detections both analytically and via Monte Carlo simulations. A closely related data analysis activity has been the search for a statistical excess of high signal-to-noise ratio (SNR), but subthreshold, CBC candidate events coincident with short GRBs. In Sec. V, we predict the science yield from searching for such statistical excesses, and demonstrate that the extra information will typically be negligible. Finally, in Appendix A, we derive a number of useful analytic formulas for describing a detector network's sensitivity to a CBC at a given sky location (i.e., the location of a GRB).

We note that rates of short GRB-GW coincident detections were also estimated in recent papers by Chen and Holz [6], and another by Kelley *et al.* [7], which appeared when this paper was almost finished. Our method is similar to both of theirs. Our conclusions are qualitatively similar to those of Ref. [6], but are qualitatively different from Ref. [7] due to different assumptions and approximations: Refs. [6,7] both assume a Gaussian distribution of outliers, while we base our calculations on the distribution of

outliers observed in the Laser Interferometer Gravitational Wave Observatory (LIGO)'s sixth and Virgo's second and third science runs (S6/VSR2,3). Reference [7] also adopts a fiducial value for the GRB jet angle that is a factor ~2 smaller than ours. (Both values are plausible, given the uncertainties.) Because of our different assumptions about the statistics of the GW search and the GRB jet angle, we derive a GRB-GW detection rate that is ~20 times higher than theirs, which lifts it from ~1/10 yr to ~2/yr (i.e., from almost negligible to interesting). Nissanke *et al.* [8] perform a similar investigation but focus on the detectability of optical counterparts to GW triggers rather than of GW counterparts of electromagnetic (EM) triggers. However, their simulations do encompass the targeted, EM-triggered GW search scenario, in their tables and figures denoted by the label *Net5b*. They predict approximately the same number of GRB-GW detections as we do, because although they assume a steeper reduction in SNR threshold relative to an all-sky GW search, they also assume a smaller GRB jet opening angle.

A. Science motivation

The detection of GWs from CBCs will have several scientific implications. The masses of the two compact objects will be determined quite accurately [9,10]. With sufficiently high SNR, the spins of these objects can also be constrained [11]. These measurements, and the overall rates, will provide information on stellar evolution [12]. The details of the late inspiral and postmerger gravitational waveform will also inform the high-density NS equation of state [13,14]. Details of the merger will also permit tests of general relativity in the strong field regime [15], tests of local Lorentz invariance [16], and constraints on the graviton mass [17,18].

A coincident short GRB-GW detection would prove that at least some GRBs are indeed produced by merger events. Furthermore, it should be possible to determine the redshift of the short GRB's host galaxy, while the GWs accurately encode the distance to the binary. It has been shown that ten short GRBs with redshift measurements could constrain H_0 to within 2%, assuming a GRB jet angle of 20° [19].

B. Recent results

To date, two types of searches for CBC signals associated with short GRBs have been executed: single-event targeted analyses for short GRBs associated with very nearby galaxies (GRBs 070201 and 051103; Refs. [3,20]), and analyses covering all short GRBs during LIGO and Virgo data-taking epochs [5,21]. None of these analyses found a significant GW candidate, but the results were used to establish lower limits on the distances, assuming CBC progenitors.

Gamma-ray bursts 070201 and 051103 had localizations that significantly overlapped with the galaxies M31 (Andromeda, 770 kpc away; Refs. [22,23]) and M81 (3.6 Mpc away; Ref. [24]), respectively. However, searches in contemporaneous GW data were able to exclude CBCs as the source of those bursts [3,20].

The 22 short GRBs that occurred during LIGO's fifth and Virgo's first science runs (S5/VSR1) were followed up with CBC searches in the GW data, using analysis methods similar to those for GRBs 070201 and 051103 [5]. The 26 short GRBs that occurred during S6/VSR2,3 were also followed up [21], using an improved, coherent analysis strategy [25]. No coincidences were found, and lower distance limits on putative CBC counterparts were established. In the more sensitive S6/VSR2,3 search, the median 90%-confidence lower limits for NS-NS and NS-BH binaries were 16 and 28 Mpc, respectively. Both analyses included a test for a subthreshold population excess. For S5/VSR1, a Mann-Whitney U test [26] was used, while a binomial test was used for S6/VSR2,3. In both cases, the subthreshold populations were found to be consistent with the background.

II. DETECTOR NETWORK ROADMAP

To make sensible predictions of the outcome of future GRB-triggered GW searches, one needs to know what GRB and GW detectors might be operating in the next decade.

A. GW detector network roadmap

The U.S. LIGO [27] has recently completed a one-year data-taking period between July 2009 and October 2010, in coincidence with the French-Italian Virgo detector [28].

LIGO is currently upgrading to its advanced detector configurations [29], with the goal of increasing the sensitivity gradually to a factor of ~10 compared to the initial configuration and extending seismic-limited sensitivity to lower frequencies. More recently, the U.S. National Science Board has authorized one LIGO detector to be moved to India in order to vastly expand the worldwide detector network's sky localization capabilities. The earlier attempts to do the same in Australia have been formally abandoned.

Virgo is upgrading to the Advanced Virgo configuration [28], similar to Advanced LIGO in optical layout and sensitivity. The start of the data-taking period with the advanced detectors is foreseen in ~2015.

GEO600 is a British-German detector with 600 m arms and advanced optical configurations [30]. GEO600's next-generation configuration will be GEO-HF with a focus on high-frequency sensitivity [31]. GEO-HF's high-frequency sensitivity will be the best in the world, which will be useful in parameter estimation [14]. However, low-frequency sensitivity is more important for CBC detection, and GEO600's relatively short arms put it at a significant disadvantage. It will likely not be used for detection searches.

Construction has begun on KAGRA (KAmioka GRAvitational wave observatory, formerly LCGT) in Japan [32], which should reach its design sensitivity in

2018. It has 3 km arms constructed underground and uses cryogenically cooled sapphire mirrors for test masses. The final detector is expected to detect a NS-NS system at a distance of 240 Mpc with SNR = 10 [33].

B. GRB detector network roadmap

During the last S6/VSR2,3 science run, the triggers came mostly from the *Swift* and *Fermi* missions, with a few from the Interplanetary Network (IPN). IPN detected most of the *Swift/Fermi* triggers too, but with a much poorer sky localization, because only triangulation methods can be used by IPN.

IPN has unfortunately lost its primary funding, but is nonetheless expected to operate during 2015–2020, if perhaps with a smaller number of satellites, still detecting GRBs at these times but with a lower rate [34]. *Swift* might operate for another five years or even longer, since it has no expendables and the spacecraft is in good shape [35], but the operation depends on NASA funding. The *Fermi* instruments might also operate until ~2018. The Gamma-ray Burst Monitor (GBM) instrument on *Fermi* achieves instantaneous sky coverage of about 70% or 8.8 sr (30% of the sky being occulted by the Earth at the altitude of Fermi's orbit; Ref. [36]), but GRBs detected by the GBM alone are very poorly localized.

Lobster is a proposed NASA mission similar to *Swift* in strategy, with a wide-field x-ray imager (WFI), a narrow-field follow-up IR telescope (IRT), and a slewing apparatus to point the latter [37]. The WFI is more sensitive than the *Swift* Burst Alert Telescope (BAT), but has a smaller field of view (FOV) at 0.5 sr.

The French-Chinese space-based multiband astronomical Variable Objects Monitor (*SVOM*) mission is targeted at a broader scientific target, including answering questions related to GRBs, cosmology, and fundamental physics [38]. Its main instrument, ECLAIR, is a coded-aperture telescope aimed at a broad energy range of 4–250 keV, with a FOV comparable to that of *Swift*. The effective detection area is also close to that of *Swift*, resulting in an expected 70–90 GRBs per year, of which 20%–25% could be short GRBs. As the ECLAIR telescopes are more sensitive to lower energies compared to BAT, the extended emission and afterglows of GRBs can be observed more deeply, resulting in improved GRB locations, and hence in a larger number (~ 50%) of GRBs with redshift measurements [39]. The anticipated launch date is ~2015–2020.

The South Korean-led Ultrafast Flash Observatory Pathfinder (UFFO-P) mission intends to catch the rise of GRBs [40]. It has been constructed and is anticipated to launch in June 2013. It carries a coded-aperture burst alert telescope similar to *Swift*'s BAT, sensitive from 15–200 keV and with a FOV of ~2 sr. UFFO-P's headlining feature is that it can repoint in response to a trigger in ~1 s using its slewing mirror telescope (SMT), which is a substantial improvement in response time over *Swift*'s ~1 minute to slew the whole spacecraft. Though UFFO-P has a small collecting area and only a small optical telescope for follow-up, this pathfinder mission already has some discovery potential. The conceived *UFFO-100* mission will increase collecting area, replace the SMT with a still faster MEMS micromirror array to redirect its optical path, and add a NIR camera, with the goal of gathering a statistically significant population of rising GRBs.

In conclusion, several missions are expected to operate during the advanced detector area, which are either already operating (like *Swift*, *Fermi* and IPN3), in development (like *SVOM* and UFFO-P), or planned (like *Lobster* and *UFFO-100*). However, given the uncertainty in how many of these missions will ultimately fly, throughout this paper we will assume that during the advanced GW detector era the effective coverage of the combined GRB detector network will be approximately that of *Swift*'s BAT alone, 1.4 sr [41], or about one tenth of the sky.

III. DETECTION PROSPECTS

A. Collimation

Gamma-ray bursts show strong evidence for collimated, relativistic outflow along a jet. Assuming that the jet is roughly conical, its size is described by the jet angle θ_j, from the center to its outer edge. We define f_b to be the fraction of the sky into which gamma rays are launched. For a CBC that emits a single jet, this is $f_b = (1 - \cos\theta_j)/2$. If the CBC emits two jets, presumably in opposite directions, then this fraction doubles to $f_b = (1 - \cos\theta_j)$. Collimation reduces the number of CBCs that are observable as short GRB events, since the observer only sees the GRBs for which the Earth lies within the jet.

The Lorentz factor Γ of the beam decreases as it sweeps up external material, and at the point where Γ reaches $\sim 1/\theta_j$, the flux decay abruptly steepens due to special relativistic effects. The beaming half-angle can be determined for a given GRB by the time of this "jet break." However, the rapid decay of the late-time light curves of short GRBs makes the estimation of θ_j difficult. Grupe *et al.* [42] place a lower limit of $\theta_j \gtrsim 25°$, while Burrows *et al.* [43] infer the value of θ_j to be in the range 4°–8°. Goldstein *et al.* [44] suggest a value in the range between 40° and 90°. Fong *et al.* [45] find 3°–8° in a recent short GRB. Simulations of NS-BH mergers indicate a range of $\theta_j \simeq 30°$–$50°$ for binaries of moderate spin, while finding 5°–10° for near-extremal spinning systems [46]. In this paper we will adopt $\theta_j = 20°$ as a fiducial value when quoting results; however, our analytic estimates and tables allow the reader to trivially convert the results to other values of θ_j.

The GRB beaming angle is presumably not a universal constant, but it has a distribution. While our simulations assumed that all GRBs had the same value for f_b, our results on rates in this paper are approximately generalizable

by simply replacing f_b with its average value $\langle f_b \rangle$. We emphasize that $\langle f_b \rangle$ refers to the average over all short GRBs, not just the detected ones, since the detected population depends on selection effects. (E.g., the detected population is biased towards GRBs with larger values of f_b, at fixed flux.)

B. Reduced search space

The search for a GW CBC signal triggered on an EM counterpart has sensitivity advantages over an all-sky search. Semianalytic calculations and numerical simulations predict that the majority of the NS matter is accreted within milliseconds to seconds. This has guided GRB-triggered CBC detection efforts to search only a $[-5, 1]$ s "on-source window" surrounding a GRB trigger to account for up to a five-second GRB-GW delay and up to 1 s of uncertainty in the GRB time of arrival (TOA) (see Secs. 2.2 and 5.1 of Ref. [21] for references). There are further possible reductions in the searched parameter space due to the known sky location, and even by restricting to the space of CBC parameters that allow for tidal disruption outside the innermost stable circular orbit, but in this paper we will neglect them, as they have much less impact than the reduction in observation time.

In this section, we are interested in estimating the reduction in SNR threshold in going from an all-sky search to a GRB-triggered search while keeping constant the false-alarm probability (FAP) at the detection threshold. The first detection is likely to be held to a high standard of FAP $\lesssim 10^{-6}$, but once detections are routine, the threshold should be lessened considerably. Throughout this paper, we assume that FAP $\lesssim 10^{-4}$ is required.

For 20 short GRBs per year of lifetime ($T_{\rm all} = 1$ yr), the observation time for GWs is $T_{\rm grb} = 120$ s. Assuming that the searches are comparably effective at background rejection, the false-alarm rate (FAR) at a given SNR should be the same, but the FAR at a given SNR, $\mathrm{FAP}(\rho) = T\mathrm{FAR}(\rho)$, is reduced by a factor

$$\frac{\mathrm{FAP}_{\rm grb}(\rho)}{\mathrm{FAP}_{\rm all}(\rho)} = \frac{T_{\rm grb}}{T_{\rm all}} \approx 4 \times 10^{-6}.$$

We have estimated the SNR threshold for a GRB-triggered search using the background SNR distribution from the S6/VSR2,3 all-sky search [47]. The all-sky search was a *coincident* search, in which matched filtering and thresholding were performed on individual detectors, and spurious triggers were vetoed by demanding consistent TOAs in multiple detectors. For a targeted GRB-triggered search, a *coherent* search is possible in which thresholding is done on the suitably time-delayed and summed SNR for the whole network [25]. False-positive rejection is aided by tests on null streams, which are special linear combinations of the detectors that are insensitive to GWs. Coherent searches are less feasible for all-sky searches, because each sky location requires unique time delays. Since in Gaussian noise a coincident search with a two-detector network has the same statistics as a coherent search with any network of (more than one) detectors [25], we can extrapolate the threshold for a targeted, coherent search from the statistics of an all-sky, coincident search.

For the S6/VSR2,3 all-sky search, Fig. 3 of Ref. [47] gives the FAR as a function of ρ_c, a χ^2-weighted quadrature sum of the SNR in all of the detectors that has been found to be a useful detection statistic. We assume that this ρ_c is equivalent to the network coherent SNR ρ, as argued above. From this figure, we find that during S6/VSR2,3, $\mathrm{FAR} = 10^{-4}\ \mathrm{yr}^{-1}$ when $\rho_c = 11.3$. When $\mathrm{FAR} = 10^{-4}/120$ s, $\rho_c = 9$. From this, we take $\rho_{\rm th,all} = 11.3$ as the SNR threshold for an all-sky search and $\rho_{\rm th,grb} = 9$ as the SNR threshold for a GRB-triggered search. A triggered search can see $11.3/9$ times farther than the all-sky search. On the other hand, as we will see, the increased range is somewhat offset by jet collimation and the limited FOVs of high-energy satellites.

IV. RESULTS

A. Analytic estimates

Here we provide some simple estimates of the CBC detection rate we expect for triggered searches, compared to the CBC detection rate for untriggered, all-sky searches. The method is the same as in Kochanek and Piran [48], but our inputs and conclusions are different. We will assume that short GRBs come *only* from CBCs, and denote by $f_{\rm GC}$ the fraction of CBCs that produce short GRBs. For the CBCs that produce bursts, let f_b be the average solid angle into which gamma rays are launched. Again, the average is over the whole GRB population, not just the population of detected GRBs (which is biased towards GRBs with wider beams at fixed flux). For any CBC that produces two beams (presumably in opposite directions), we consider f_b for *that* burst to be the sum of the solid angles for the two beams. Finally, we define $\bar{S}$ to be the average fraction of the sky that is "covered" by the then-existing GRB detector network. For the advanced GW detectors, most CBCs will be detected at distances $\lesssim 200$ Mpc, while most detected short GRBs are much farther away ($D \sim 1$ Gpc), so the GRB accompanying an observed CBC should be detectable as long as the Earth lies within the beam, and the source is within the telescope's FOV. Then the fraction F of CBCs for which we detect a GRB is

$$F = f_{\rm GC} \bar{S} f_b. \tag{1}$$

We shall adopt $F = 6 \times 10^{-3}$ as a reasonable fiducial number. This would correspond, e.g., to $\bar{S} = 0.1$, and all CBCs emitting two jets of $\theta_j = 20°$ each.

As explained above, by looking for NS binaries that are roughly coincident in time with observed short GRBs, we increase the sensitivity of the search at fixed FAR. Let

$\rho_{\rm th,all}/\rho_{\rm th,grb}$ be the ratio of the GW detection thresholds for blind and GRB-triggered searches, respectively. As explained in Sec. III B, we adopt as a fiducial value $\rho_{\rm th,all}/\rho_{\rm th,grb} \approx 11.3/9.0 \approx 1.25$.

The final factor that we need arises because the mergers that we see in gamma rays are presumably the ones for which we are viewing the binary nearly face on (because the gamma rays are presumably beamed perpendicular to the orbital plane.) The quadrupolar pattern of the emitted GWs is also strongest along the direction perpendicular to the orbital plane; the amplitude of h on the axis is ≈ 1.51 times stronger than the isotropic detection-averaged value. (It is well know that that rms enhancement is $\sqrt{5/2} = 1.58$, but what is relevant for determining rates is the cube root of mean-cubed enhancement, which is 1.51.) Although 1.51 is the enhancement factor of an optimally oriented binary, we show in Appendix A that as long as the beam half-angle is $<25°$, then using 1.51 is at most a $\sim$5% overestimate, which is acceptable for our purposes.

For Advanced LIGO, we will be detecting CBCs in the range $\sim$50 Mpc to $\sim$500 Mpc. At these distances, we can safely approximate spatial geometry as Euclidean and the density of mergers as uniform. Let $\dot{\mathcal{N}}_{\rm all}$ be the CBC detection rate of blind, all-sky advanced GW detector searches, and let $\dot{\mathcal{N}}_{\rm grb}$ be the rate for triggered searches. What is the ratio $\dot{\mathcal{N}}_{\rm grb}/\dot{\mathcal{N}}_{\rm all}$? The volume in which GRB-triggered CBCs are detectable is larger than for the blind case by the factor $(1.51\rho_{\rm th,all}/\rho_{\rm th,grb})^3$, but recall that only a fraction F of the CBCs emit detectable gamma rays. Thus,

$$\frac{\dot{\mathcal{N}}_{\rm grb}}{\dot{\mathcal{N}}_{\rm all}} = \left(1.51\,\frac{\rho_{\rm th,all}}{\rho_{\rm th,grb}}\right)^3 F \sim 0.041. \tag{2}$$

In other words, of the first $\sim$25 detections, we would expect only one to come from the GRB-triggered pipeline; it is correspondingly unlikely that the very first GW detection of a CBC will result from a GRB trigger. This is the same conclusion reached in Chen and Holz [6] and Kelley *et al.* [7].

Of the CBC detections associated with short GRBs, a fraction $(\rho_{\rm th,all}/\rho_{\rm th,grb})^3 \sim 0.5$ will be strong enough to be detectable even without the GRB trigger. So the *increase* in the rate of GW detections, thanks to GRB triggers, will be $\sim$2%. This is a small increase in CBC detections, but, given the extra information to be gleaned from the EM counterpart, a non-negligible one. Note that this 2% increase is about 2 times higher than the fiducial increase reported in Kelley *et al.* [7]. The difference comes mostly from two factors: i) a factor $\sim$4–5 from our use of non-Gaussian statistics, and ii) a factor $\sim$6–7 from our wider fiducial beam angle of 20° vs their 11°, combined with our assumption of two opposite-pointing jets per CBC.

B. Effective sensitive volumes

For a given detector network and mass pair, we would like to compute the relative detection capability of a targeted short GRB search compared to an all-sky search. Following Finn and Chernoff [10], but generalizing from a single detector to a network, we define an effective sensitive volume $V_{\rm sens}$, which can be multiplied by a constant rate density $\mathcal{R}$ to obtain the total detection rate $\dot{\mathcal{N}} = \mathcal{R} V_{\rm sens}$:

$$\begin{aligned} V_{\rm sens} &= \left\langle \int \Theta(\rho - \rho_{\rm th}) dV \right\rangle_{\psi,\iota} \\ &= \int d\Omega \left\langle \int_0^{D_{\rm th}} r^2 dr \right\rangle_{\psi,\iota} \\ &= \frac{4\pi}{3} \langle D_{\rm th}^3 \rangle_{\psi,\iota,\delta,\alpha}, \end{aligned} \tag{3}$$

where Θ is the Heaviside step function, (α, δ) are the source's right ascension and declination, and $D_{\rm th}$ is the distance at which the network registers SNR above its threshold $\rho_{\rm th}$ for a given source type. $D_{\rm th}$ depends on the full specification of a waveform plus the detector noise spectrum and the various projection angles. Equation (3) is quite convenient for Monte Carlo integration. See Appendix A for network SNR expressions and analytical evaluation of Eq. (3) in the nonspinning case.

To take into account the imperfect duty cycle of the detectors, along with our requirement that at least two detectors be "on" to claim a detection, it is useful to define a *double detection volume* (2DV), in close analogy to the triple detection rate (3DR) of Schutz [49]. (Our formulation generalizes the treatment in Schutz [49], since it applies to spinning binaries and removes the assumption of equal detector responses.) For a set of detectors $\mathcal{N}$,

$$\mathrm{2DV} = \sum_{\mathcal{X} \in \mathcal{P}_{\geq 2}(\mathcal{N})} f^{|\mathcal{X}|}(1-f)^{|\mathcal{N}|-|\mathcal{X}|} V_{\rm sens}^{\mathcal{X}}, \tag{4}$$

where $\mathcal{P}_{\geq 2}(\mathcal{N})$ is the set of subsets of $\mathcal{N}$ with size 2 or greater and $|\mathcal{X}|$ denotes the size of set $\mathcal{X}$. The value f is the duty cycle, which we take to be the same for all detectors.

C. Results from simulations

We evaluate the 2DV [Eq. (4)] via Monte Carlo integration, randomly drawing the sky location and the polarization angles, for both NS-NS (1.4-1.4$M_\odot$) and NS-BH (1.4-10$M_\odot$) pairs. We use the Taylor T4 waveform [50], including general spin precession, to determine expected signal amplitudes, and thus $D_{\rm th}$. We match the distributions of spin amplitude and spin orientation used in the recent GRB 051103 analysis [20] with NS dimensionless spin drawn uniformly from [0, 0.4], BH spin drawn uniformly from [0, 0.98], and uniform spin orientations subject to a cut on the tilt angle (the angle between the BH spin axis and NS orbital axis) to be $<60°$. We also adopt their rigid

TABLE I. Double detection volume (2DV) in Gpc^3.

	NS-NS		NS-BH	
θ_j	$V^9_{\theta_j}$	$V^{11.3}_{\theta_j}$	$V^9_{\theta_j}$	$V^{11.3}_{\theta_j}$
10	0.31	0.16	2.5	1.3
20	0.29	0.15	2.4	1.2
30	0.26	0.13	2.1	1.1
40	0.23	0.11	1.9	0.95
50	0.19	0.097	1.6	0.81
60	0.16	0.080	1.3	0.68
70	0.13	0.066	1.1	0.57
80	0.11	0.056	0.96	0.48
90	0.093	0.047	0.83	0.42

rotation procedure so that it is the total angular momentum that is uniformly distributed within the cone of θ_j rather than the orbital angular momentum. Using different values for θ_j, we compute the relative improvement in effective sensitive volume 2DV of a triggered search (restricted inclination angle, coherent threshold $\rho_{\mathrm{th,grb}} = 9.0$) compared to an all-sky search (unrestricted inclination, coincident threshold $\rho_{\mathrm{th,all}} = 11.3$).

The 2DVs have been defined such that the detection rate for the all-sky search is $\dot{\mathcal{N}}_{\mathrm{all}} = \mathcal{R}V^{11.3}_{90^\circ}$, where $\mathcal{R}$ is the merger rate density in the local Universe, and $V^{11.3}_{90^\circ}$ is the 2DV assuming a coherent SNR threshold of 11.3 and a source population whose inclination is unrestricted ($\theta_j = 90^\circ$). Similarly, the number of GRBs associated with a GW detection is given by $\dot{\mathcal{N}}_{\mathrm{grb}} = \bar{S}f_b\mathcal{R}V^9_{\theta_j}$. The rate for GRBs independently detected by both searches (i.e., with GW network SNR > 11.3) is $\dot{\mathcal{N}}_{\mathrm{both}} = \bar{S}f_b\mathcal{R}V^{11.3}_{\theta_j}$. Our computed sensitive volumes are shown in Table I. Each value of $V^9_{\theta_j}$ represents 10^6 simulations, while the $V^{11.3}_{\theta_j}$ values are simply rescaled from $V^9_{\theta_j}$.

TABLE II. Annual detection rate of short GRB-CBC coincidences by the externally triggered search ($\dot{\mathcal{N}}_{\mathrm{grb}}$), and by both the triggered search and the all-sky search ($\dot{\mathcal{N}}_{\mathrm{both}}$). For comparison, we compute the annual detection rate for CBC signals, with or without GRB counterparts, by the all-sky search ($\dot{\mathcal{N}}_{\mathrm{all}}$) to be 61 and 18 for NS-NS and NS-BH sources, respectively.

	NS-NS		NS-BH	
θ_j	$\dot{\mathcal{N}}_{\mathrm{grb}}$	$\dot{\mathcal{N}}_{\mathrm{both}}$	$\dot{\mathcal{N}}_{\mathrm{grb}}$	$\dot{\mathcal{N}}_{\mathrm{both}}$
10	0.62	0.31	0.16	0.083
20	2.3	1.2	0.61	0.31
30	4.6	2.3	1.2	0.62
40	6.9	3.5	1.9	0.95
50	8.9	4.5	2.5	1.2
60	10	5.2	2.9	1.5
70	11	5.7	3.2	1.6
80	12	6.0	3.4	1.7
90	12	6.1	3.6	1.8

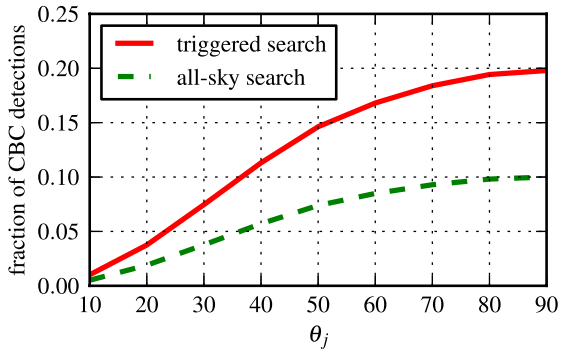

FIG. 1 (color online). Fractional number of additional CBC detections contributed by an externally triggered search (solid) and fraction of all-sky CBC detections predicted to be in coincidence with short GRB observations without a special triggered search (dashed). NS-NS and NS-BH ratios are equal within statistical uncertainty, so only NS-NS results are plotted.

Under the assumption that all CBCs produce short GRBs and vice versa, we translate sensitive volumes to detection rates in Table II and Fig. 1. We take values of $0.0198L_{10}/\mathrm{Mpc}^3$ and "realistic" coalescence rates of $6 \times 10^{-5}L_{10}^{-1}\,\mathrm{yr}^{-1}$ for NS-NS sources and $2 \times 10^{-6}L_{10}^{-1}\,\mathrm{yr}^{-1}$ for NS-BH sources, as used in Abadie *et al.* [51]. The coalescence rates are uncertain by 2 orders of magnitude, but our relative volumes have much smaller errors, so we show two or more significant figures not to reflect uncertainty but rather to allow for relative comparisons. We have assumed an effective FOV of $\bar{S} = 0.1$, independent duty cycle factors of $f = 0.8$, and a network of LIGO-Hanford, LIGO-Livingston, Virgo, KAGRA (final orientation via Ref. [52]), and LIGO-India (HLVKI; orientation guess via Ref. [49]). For all GW detectors, we used publicly available projections of noise spectra at full design sensitivities [53–55]. However, we started SNR integration from a lower frequency limit of 40 Hz in order to fit waveforms within the memory limits of the bulk of computers available to us, enabling much greater parallelism, at some cost in realism. These assumptions lead to a total annual detection rate of 61 NS-NS signals and 18 NS-BH signals for the all-sky search.

Assuming an effective FOV of $\bar{S} = 0.1$ for the GRB detectors, and that every CBC produces two opposite jets, each with a fiducial jet angle of $\theta_j = 20^\circ$, we find that 1.8% of CBCs detected by the all-sky search would be coincident with observed short GRBs. Adding the triggered search increases the number of coincidences to 3.8%. Clearly, our Monte Carlo results are in very close agreement with the analytic estimates in Sec. IV A.

V. SUBTHRESHOLD STATISTICAL EXCESS TESTS

In a calendar year, there will be some number of searches for GWs associated with short GRBs. Some of these may result in individual detections, meaning that

there will be events that survive all vetoes and have SNR above some theshold ρ_1 for confident single-source detection. However, one can also consider some lower threshold ρ_e, and look for a statistical excess of events with SNR between ρ_e and ρ_1. What science can be gleaned from those excess events?

We begin by providing a Bayesian perspective on this question. First, setting any threshold and discarding events below that threshold amounts to ''throwing away'' data, and in the ideal case of arbitrary computing power and a perfectly known distribution of the detection statistic, discarding data weakens the analysis. So in the ideal case, ρ_e would be set very low. However, in practice, finite resources, an imperfectly known distribution of outliers, and diminishing infomation returns (for lower ρ_e) all will push data analysts to a value of ρ_e not too far below ρ_1. Probably the most important information encoded in the excess, sub-ρ_1 events is an improved estimate of the event rate $\mathcal{R}$ (e.g., in units of $\mathrm{Mpc}^{-3}\,\mathrm{yr}^{-1}$). As emphasized in Messenger and Veitch [56], a proper Bayesian analysis takes into account the value of ρ_e, and so always gives an unbiased estimate of $\mathcal{R}$. Including more events by lowering ρ_e just ''shrinks the error bars.''

Next, we provide a crude, back-of-the-envelope argument why, in the regime of rare detection, there will generally not be much information in the subthreshold excess. In the regime of rare detection, the unique loudest event will have SNR ~ 10. There are 8 times as many events twice as far away, so we would expect an order of 8 true events with $5 < \mathrm{SNR} < 10$. However, the number of background events with SNR between 5 and 10 will be of order 10^{-4} (the FAP at SNR ~ 10) times $e^{-25/2}/e^{-100/2}$, or $\sim 10^{12}$ (assuming a Gaussian distribution of noise events). The standard deviation in this expected number of events is 10^6, which swamps the true excess. Of course, this calculation was for one (nonoptimized) value of ρ_e, but we believe that the general conclusion is robust: as ρ_e is decreased below ρ_1, the background rate increases far faster than the rate of true events, so we expect relatively little extra information from the subthreshold events.

In the next subsection, we consider two non-Bayesian statistical excess tests currently used in LIGO searches, and show through simulations that, indeed, the sub-ρ_1 excess typically contains rather little useful information. We believe that a proper Bayesian analysis of the sub-ρ_1 events would lead to the same qualitative conclusion, but we leave that calculation for future work.

A. Results from simulations

In past LIGO searches, two statistical excess tests were employed: the Mann-Whitney-Wilcoxon U test, and later the binomial test [5,21]. However, we are not aware of any systematic comparison of their detection power, so we compare them here.

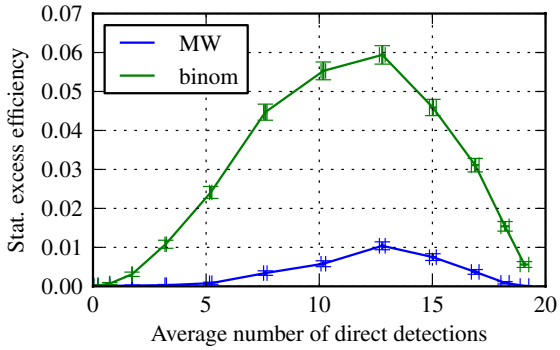

FIG. 2 (color online). Fraction of simulations in which the U and binomial tests detected a statistical excess in subthreshold candidates vs the rate of direct detections.

We ran a Monte Carlo simulation in which each trial drew 20 GRB on-source candidates and, for each one, 10^6 off-source trial loudest candidates. Off-source candidates were drawn from the S6/VSR2,3 distribution (see Sec. III B). Each on-source candidate SNR was the maximum of an off-source trial and a draw from a foreground $p(\rho) \propto \rho^{-4}$ distribution whose rate scaling could be varied. For each trial, we performed individual direct detection searches on all 20 GRBs before performing a statistical excess search on the set of remaining nondetections. Both direct detection of individual GRBs and statistical excess detection had thresholds set by FAP $= 10^{-4}$. Figure 2 shows the fraction of trials in which the U and binomial tests were able to detect an excess vs the average number of direct detections among the 20 simulated GRBs. While the U test used all on-source and all off-source candidates, the binomial considered only the loudest four on-source candidates.

We see our expectations confirmed: for both tests, the probability of detecting an excess in the subthreshold population is never larger than several percent. Of the two tests, the binomial one is the more powerful. We see both tests become more powerful as the number of direct detections rises, until it reaches $\sim$13. The decline in efficiency for $>$13 detections is an artifact of the ''rules'' of our simulation in that there are always 20 true events, so as more of them exceed ρ_1, fewer true events are left among the subthreshold candidates.

VI. SUMMARY AND DISCUSSION

Based on LIGO and Virgo S6/VSR2,3 data and search parameters for CBC-short GRB searches, we have quantified how much deeper into the noise one can dig with knowledge of the external trigger time; we find a coherent SNR threshold of 9.0 vs an all-sky coincident threshold of 11.3 for a detection FAP of 10^{-4}. References [6,7] have also estimated the reduction in the SNR threshold assuming Gaussian noise and making different choices in how to fold in EM information. The bleakness of Ref. [7]

compared to our study is easily understood: if the measured distribution of SNRs falls off less steeply than a Gaussian, then reducing the search volume has a relatively larger effect on the detection threshold (at fixed FAP), and hence on the detection rate. While the advanced detectors will not have the same distribution of high-SNR candidates SNRs as LIGO and Virgo did in S6/VSR2,3, the true distribution seems unlikely to be Gaussian, and the difference between our results and Refs. [6,7] provides some measure of the importance of non-Gaussian backgrounds in assessing the value of triggered searches.

Folding the threshold reduction into a large Monte Carlo simulation, including the effects of short GRB collimation, general spin precession, and advanced GW and GRB detector networks, we have estimated the rate of CBC-short GRB coincident detections. Assuming that all NS-NS systems produce short GRBs with a jet angle of 20°, we find that, relative to just an all-sky search, adding a search triggered by a *Swift*-like satellite increases the total number of CBC detections by 2%, but more importantly doubles the number of GW-GRB associations. A mission such as *Fermi* that has ~6 times the instantaneous sky coverage of *Swift* would contribute not quite an increase of ~12% to the total number of CBC detections, because the relatively poor sky localization would permit less of a reduction in the GW detection threshold. Although the calculated enhancement of detection rate is dependent on this and other assumptions, we believe it justifies the effort that is being spent on such triggered searches, given the extra scientific value of multimessenger detections.

The externally triggered GRB searches to date have attempted to detect a population of subthreshold GWs. We performed simulations that show that typically there will not be a detectable excess until the rate of direct detections of individual sources is already high; hence, it is highly unlikely that an excess population test will provide the first strong evidence for CBCs.

ACKNOWLEDGMENTS

The authors thank Alan Weinstein and Michal Was for comments on the manuscript, and Neil Gehrels for updating us on GRB missions. LIGO was constructed by the California Institute of Technology and Massachusetts Institute of Technology with funding from the National Science Foundation (NSF) and operates under cooperative agreement No. PHY-0107417. L. S. is supported by the NSF through a Graduate Research Fellowship, while A. D. is supported by NSF Grants No. PHY-1067985 and No. PHY-0757937. C. C.'s work was carried out at the Jet Propulsion Laboratory, California Institute of Technology, under contract to the National Aeronautics and Space Administration. C. C. also gratefully acknowledges support from NSF Grant No. PHY1068881. This paper has LIGO Document No. LIGO-P1200113- v7.

APPENDIX A: PRIOR DISTRIBUTION OF A GW DETECTOR NETWORK'S RESPONSE TO A CBC AT A GIVEN DISTANCE AND SKY LOCATION

In this section, we discuss the distribution of a network's response to GWs from a source at a particular, known sky location and distance, whose orientation is unknown but whose inclination is restricted to be less than a maximum value $\iota_{\max} = \theta_j$. When studying an individual GRB, we could treat this as a prior distribution for the strength of the signal received by a particular detector network. In the event of a nondetection, it would allow us to parameterize the excluded distance by the jet opening angle.

Let the frequency domain GW strain received by detector X be $h^X(f)$ and the noise power spectral density of detector X be $S^X(f)$. Defining the inner product

$$(r^X)^2 = \langle h^X, h^X \rangle = 4\,\mathrm{Re}\int_0^\infty \frac{(h^X)^*(f)h^X(f)}{S^X(f)}\,\mathrm{d}f$$

and then the sum over all of the detectors

$$r^2 = \sum_X (r^X)^2,$$

the coherent detection statistic ${\rho_{\mathrm{coh}}}^2$ defined by Harry and Fairhurst [25] and the incoherent, coincident detection statistic ${\rho_{\mathrm{coinc}}}^2$ are noncentrally chi-squared distributed with the noncentrality parameter given by r^2. (The coherent detection statistic has 4 degrees of freedom, whereas the coincident statistic has 2 degrees of freedom times the number of detectors.) We will first derive summary statistics of r: its minimum, maximum, mode, mean, and root-mean-square (rms). Then, we will derive the full distribution of r and study its qualitative features.

Harry and Fairhurst [25] introduce D, the luminosity distance of the source; D_0, an arbitrary fiducial distance; the three angles (ι, ψ, ϕ_0) describing the orientation of the source, being respectively the inclination of the orbital plane to the line of sight, the polarization angle, and the orbital phase at coalescence; and the antenna factors of each detector, F_+^X and $F_\times^X$, which are functions of sky location. They also define two waveform quadratures, h_0 and $h_{\pi/2}$, which are nearly orthogonal such that

$$4\int_0^\infty \frac{|h_0(f)|^2}{S^X(f)}\,\mathrm{d}f \approx 4\int_0^\infty \frac{|h_{\pi/2}(f)|^2}{S^X(f)}\,\mathrm{d}f = (\sigma^X)^2$$

and

$$4\mathrm{Re}\int_0^\infty \frac{h_0^*(f)h_{\pi/2}(f)}{S^X(f)}\,\mathrm{d}f \approx 0.$$

They define a further three quantities that combine the antenna factors of a network of detectors:

$$\left.\begin{aligned} A &= \sum_X (\sigma^X F_+^X)^2 \\ B &= \sum_X (\sigma^X F_\times^X)^2 \\ C &= \sum_X (\sigma^X F_+^X)(\sigma^X F_\times^X). \end{aligned}\right\}. \quad \text{(A1)}$$

It is easily—though laboriously—shown that the detector response or noncentrality parameter r^2 depends only on the antenna factors, distance, ι, and ψ, through

$$r^2 = \frac{1}{8}\frac{{D_0}^2}{D^2}[(A+B)(x^4+6x^2+1) + \sqrt{(A-B)^2+4C^2}(1-x^2)^2\cos\alpha], \quad \text{(A2)}$$

where $x = \cos\iota$ and $\alpha = 4\psi - \mathrm{atan2}(2C, A-B)$. For the purpose of concise parameterization of r^2, we will also introduce $x_0 = \cos\iota_{\max}$, $J^2 = A+B$, and $K^2 = \sqrt{(A-B)^2+4C^2}/(A+B)$. J^2 describes the total sensitivity of the detector network as the weighted sum of squares of all of the antenna factors. To lend interpretation to K^2, we write Eq. (A1) as

$$H = \begin{pmatrix} \sigma^1 F_+^1 & \sigma^2 F_+^2 & \sigma^3 F_+^3 & \cdots \\ \sigma^1 F_\times^1 & \sigma^2 F_\times^2 & \sigma^3 F_\times^3 & \cdots \end{pmatrix} \begin{pmatrix} \sigma^1 F_+^1 & \sigma^1 F_\times^1 \\ \sigma^2 F_+^2 & \sigma^2 F_\times^2 \\ \sigma^3 F_+^3 & \sigma^3 F_\times^3 \\ \vdots & \vdots \end{pmatrix} \equiv \begin{pmatrix} A & C \\ C & B \end{pmatrix}.$$

Then, K^2 can be shown to equal the ratio of the difference of the eigenvalues of H to their sum. K^2 measures the extent to which the network is preferentially sensitive to just one polarization, in a way that is independent with respect to rotations of the detector network's coordinate system. If the network is equally sensitive to two orthogonal polarizations, then K^2 vanishes. If the network is sensitive to only one polarization, then K^2 is unity.

Lastly, we define u^2 as the distance-independent part of r^2:

$$u^2 = \left(\frac{D_0^2}{D^2}\right)^{-1} r^2 = \frac{1}{8}J^2[(x^4+6x^2+1) + K^2(1-x^2)^2\cos\alpha].$$

Our goal is to study the conditional probability density function (PDF), $p(u|\theta, \phi, \iota \le \iota_{\max})$, of u, assuming a fixed sky location and a censored orientation distribution. Under the assumption that the GRB emission is collimated within an angle $\iota_{\max} = \theta_j$, the burst can only be seen if the Earth is placed inside this cone. As the probability is the same for random placement anywhere on the surface of this cone, the prior distribution of the inclination angle ι between the line of sight to Earth and the axis of the outflow is given by

$$p(\iota) = \frac{\sin\iota}{1-\cos\iota_{\max}} \quad \text{where } 0 \le \iota \le \iota_{\max}, \quad \text{(A3)}$$

since an area element on the cone is given by $dA = \sin\iota d\iota d\phi$. This represents a prior distribution on the direction of the system's orbital axis that is uniform in solid angle, restricted to polar angles $\le \iota_{\max}$.

Having parameterized the detector network's response, we proceed to derive the distribution of r for a given sky location and luminosity distance, as well as the minimum, maximum, mean, rms, and mode of the distribution. Finally, as an example, we will apply our results to GRB 051103.

1. Distribution and summary statistics

The distribution of the detector network's response and its summary statistics, derived below, are plotted in Fig. 3 for a selection of detector networks and maximum inclination angles.

a. Minimum and maximum

The minimum value of u is obtained when the source is at the maximum inclination ($\iota = \iota_{\max}$ or $x = x_0$) and when $\cos\alpha = -1$:

$$u_{\min} = \left(\frac{J}{\sqrt{8}}\right)\sqrt{x_0^4+6x_0^2+1-K^2(1-x_0^2)^2}. \quad \text{(A4)}$$

The maximum value is obtained when the source is at the minimum inclination ($\iota = 0$ or $x = 1$):

$$u_{\max} = J. \quad \text{(A5)}$$

b. Mean

The mean response is given by

$$u_{\text{mean}} = \int_{x_0}^1 \int_0^{2\pi} \frac{J}{\sqrt{8}} \times \frac{\sqrt{(x^4+6x^2+1)+K^2(1-x^2)^2\cos\alpha}}{2\pi(1-x_0)}\,\mathrm{d}\alpha\mathrm{d}x.$$

It is possible to cast the integral over α into the form of a complete elliptic integral of the second kind,

$$u_{\text{mean}} = \frac{J}{\sqrt{2}\pi(1-x_0)}\int_{x_0}^1 \sqrt{x^4+6x^2+1+K^2(1-x^2)^2} \times E\left(\sqrt{\frac{2K^2(1-x^2)^2}{x^4+6x^2+1+K^2(1-x^2)^2}}\right)\mathrm{d}x, \quad \text{(A6)}$$

where

$$E(k) = \int_0^{\frac{\pi}{2}} \sqrt{1-k^2\sin^2\alpha}\,\mathrm{d}\alpha.$$

c. Root-mean-square

The rms response is

$$u_{\rm rms}{}^2 = \int_{x_0}^{1}\int_{0}^{2\pi}\frac{J^2}{8} \times\left[\frac{(x^4+6x^2+1)+K^2(1-x^2)^2\cos\alpha}{2\pi(1-x_0)}\right]{\rm d}\alpha{\rm d}x.$$

The integral over α kills the $\cos\alpha$ term, leaving

$$u_{\rm rms}{}^2 = \frac{J^2}{8}\int_{x_0}^{1}\left[\frac{x^4+6x^2+1}{1-x_0}\right]{\rm d}x.$$

The integral over x gives

$$u_{\rm rms} = \left(\frac{J}{2\sqrt{10}}\right)\sqrt{x_0^4+x_0^3+11x_0^2+11x_0+16}. \quad \text{(A7)}$$

d. Full probability distribution

We have the prior distribution of (ι, α),

$$p(\iota,\alpha) = \frac{\sin\iota}{2\pi(1-\cos\iota_{\rm max})} \quad \text{where } \alpha\in[0,2\pi],\ \iota\in[0,\iota_{\rm max}],$$

or equivalently,

$$p(x,\alpha) = \frac{1}{2\pi(1-x_0)} \quad \text{where } \alpha\in[0,2\pi],\ x\in[x_0,1].$$

To compute the conditional PDF of u, $p(u|\theta,\phi,\iota\le\iota_{\rm max})$, the first step is to effect a change of variables from ${\rm d}x{\rm d}\alpha$ to ${\rm d}x{\rm d}u$. To do this, we write $\mathbf{y}=\mathbf{f}(\mathbf{x})$ where $\mathbf{x}=(x,\alpha)$ and $\mathbf{y}=(x,u)$. By forming the Jacobian determinant $|\partial\mathbf{f}/\partial\mathbf{x}|$, we find

$${\rm d}x{\rm d}\alpha = \left|\begin{array}{cc}1 & 0\\ \frac{\partial u}{\partial x} & \frac{\partial u}{\partial\alpha}\end{array}\right|^{-1}{\rm d}x{\rm d}u = \left|\frac{\partial u}{\partial\alpha}\right|^{-1}{\rm d}x{\rm d}u.$$

Using the inverse rule for derivatives, $\partial y/\partial x=(\partial x/\partial y)^{-1}$, we solve for α as a function of u,

$$\alpha = \arccos\frac{8u^2/J^2-(x^4+6x^2+1)}{K^2(1-x^2)^2},$$

and then differentiate with respect to u,

$$\frac{\partial\alpha}{\partial u} = -\frac{16u}{J^2K^2(1-x^2)^2}\left[1-\left(\frac{8u^2/J^2-(x^4+6x^2+1)}{K^2(1-x^2)^2}\right)^2\right]^{-\frac{1}{2}} = -\frac{16u}{\sqrt{[J^2K^2(1-x^2)^2]^2-[8u^2-J^2(x^4+6x^2+1)]^2}}.$$

Now we may express the conditional PDF that we seek as

$$p(u|\theta,\phi,\iota\le\iota_{\rm max}) = \int_0^{\iota_{\rm max}} 2\left|\frac{\partial\alpha}{\partial u}\right| p(x,\alpha){\rm d}x.$$

The factor of 2 accounts for the two distinct values of α that give the same value of u. Altogether,

$$p(u|\theta,\phi,\iota\le\iota_{\rm max}) = \frac{16}{\pi J(1-x_0)}\int_{x_1}^{x_2}\frac{u/J}{\sqrt{[K^2(1-x^2)^2]^2-[8(u/J)^2-(x^4+6x^2+1)]^2}}\,{\rm d}x. \quad \text{(A8)}$$

We have to be a little careful about the limits of integration; the quantity in the radical must remain positive. It has a zero at

$$x^2 = \frac{-3+K^2+\sqrt{8[1-K^2+u^2(1+K^2)/J^2]}}{1+K^2}.$$

The lower limit should be

$$x_1 = \sqrt{\max\left(\frac{-3+K^2+\sqrt{8[1-K^2+(\frac{u}{J})^2(1+K^2)]}}{1+K^2}, x_0^2\right)}. \quad \text{(A9)}$$

The upper limit should be

$$x_2 = \begin{cases}\sqrt{\frac{-3-K^2+\sqrt{8[1+K^2+u^2(1-K^2)/J^2]}}{1-K^2}} & \text{if } K\neq 1\\ u/J & \text{if } K=1.\end{cases} \quad \text{(A10)}$$

Equation (A8) may be evaluated numerically using, for example, Simpson's rule.

e. Mode

The mode of the distribution occurs when the lower limit of integration ceases to clip against the minimum value, where

$$x_0 = \sqrt{\frac{-3+K^2+\sqrt{8[1-K^2+u^2(1+K^2)/J^2]}}{1+K^2}}.$$

This occurs at

$$u_{\rm mode} = \left(\frac{J}{\sqrt{8}}\right)\sqrt{x_0^4+6x_0^2+1+K^2(1-x_0^2)^2}. \quad \text{(A11)}$$

2. Special case: Unrestricted inclination

If the inclination is unrestricted, $\iota_{\rm max}=\pi/2$ or $x_0=0$, then the above results simplify to

$$u_{\rm mode} = J\sqrt{1+K^2}/\sqrt{8}, \qquad u_{\rm min} = J\sqrt{1-K^2}/\sqrt{8},$$
$$u_{\rm max} = J, \qquad u_{\rm rms} = \sqrt{2}J/\sqrt{5}.$$

Neither $u_{\rm mean}$ nor the full PDF $p(u|\theta,\phi,\iota\le\iota_{\rm max})$ simplify much for the unrestricted inclination case.

3. Special case: One detector

When the detector network consists of only one detector, $C^2 = AB$, $K = 1$, and $J^2 = \sigma^2 F^2$, where $F^2 = F_+{}^2 + F_\times{}^2$. With these substitutions,

$$
\begin{aligned}
u_{\rm mode} &= J(1 + x_0^2)/2, \\
u_{\rm min} &= J x_0, \\
u_{\rm max} &= J, \\
u_{\rm rms} &= \left(\frac{J}{2\sqrt{10}}\right)\sqrt{x_0^4 + x_0^3 + 11x_0^2 + 11x_0 + 16}, \\
u_{\rm mean} &= \frac{J}{\pi(1 - x_0)} \int_{x_0}^{1} (1 + x^2) E\left(\frac{1 - x^2}{1 + x^2}\right) {\rm d}x, \\
p(u|\theta, \phi, \iota \le \iota_{\rm max}) &= \frac{16}{\pi J(1 - x_0)} \int_{x_1}^{x_2} \frac{u/J}{\sqrt{[(1 - x^2)^2]^2 - [8u^2/J^2 - (x^4 + 6x^2 + 1)]^2}} \, {\rm d}x, \\
x_1 &= \sqrt{\max\,(2u/J - 1, x_0^2)}, \\
x_2 &= u/J.
\end{aligned}
$$

4. Case study: GRB 051103

GRB 051103 was an exceptionally short, hard, and bright burst detected by *HETE*, *Suzaku*, and *Swift*, and localized by IPN to an area consistent with the outer disc of M81 [24]. Owing to its brightness and hardness, a giant flare from an extragalactic soft gamma-ray repeater (SGR) was a plausible progenitor. The Hanford 2-km detector (H2) and Livingston 4-km detector (L1) were operating at the time, so a targeted search of the GW data was undertaken. No candidate was detected, but the nondetection excluded a CBC event in M81 as the progenitor [20]. Under the assumption that a CBC progenitor would have produced a collimated jet along the axis of strongest gravitational wave emission, Abadie *et al.* [20] placed 90%-confidence lower limits on the distance of a CBC progenitor as a function of jet angle. A collimated GRB in M81 was firmly excluded.

As an example, we apply our distribution of detector response to the problem of estimating the exclusion distance as a function of jet opening angle for GRB 051103. If we knew the GW search's detection efficiency for strictly face-on sources, then using our distribution for (u/J), we could directly calculate the excluded distance for any jet opening angle and any confidence level. Abadie *et al.* [20] did not publish that detection efficiency, but we can do a qualitatively similar calculation by extrapolating from their 90% exclusion distance for $\theta_j = \iota_{\rm max} = 10°$, attempting to reproduce their exclusion distance at other jet opening angles.

GRB 051103 occurred at 3 November 2011, 09:25:42 UTC. The H2 and L1 horizon distances (distance at which an optimally oriented face-on CBC would register an amplitude $r = 8$) at this time for both a 1.4-1.4$M_\odot$ NS-NS event and a 1.4-10$M_\odot$ NS-BH event are given in Table III, along with the antenna factors at this time in the direction of M81. For a NS-NS signal, this network has $K^2 = 0.9601$, and for a NS-BH signal, $K^2 = 0.9602$. H2 and L1 had almost the same sensitivity up to a frequency-independent factor of ≈ 2, so it is not surprising that the value of K^2 is almost the same for both the NS-NS and NS-BH signal models.

In Fig. 4, we plot the 90% exclusion distance as a function of $\theta_{\rm jet}$ from Fig. 3 of Abadie *et al.* [20]. We have superimposed the mode of the detector response distribution, Eq. (A11), scaled to match the published exclusion distance at $\theta_j = 10°$, as a dashed line. The value of (u/J) at which the cumulative distribution function (CDF) is equal to $(1 - 0.9)$ is shown as a solid line. The inverse CDF agrees well with the NS-NS exclusion distance, but the mode agrees much better with the NS-BH exclusion distance than the inverse CDF. Exact agreement is not expected with either: as we have pointed out, a proper application to calculating exclusion distances would require knowledge of both the prior distribution of (u/J) and the sensitivity of the GW search to face-on sources as a function of signal amplitude. Furthermore, the analysis of Abadie *et al.* [20] includes a Monte Carlo integration over a range of masses, whereas our analysis fixes canonical choices of the masses.

APPENDIX B: ENHANCED GW AMPLITUDE OF GRB-TRIGGERED SOURCES

In this paper, we assume that the emitted gamma rays are collimated within an angle θ_j of the normal to the orbital plane, and thus the binary inclination ι must be less than

TABLE III. Antenna factors and horizon distances for H2 and L1 detectors at the time of GRB 051103.

Detector	F_+	$F_\times$	$DH_{\rm NSNS}$	$DH_{\rm NSBH}$
H2	−0.152	−0.706	8.3	17.1
L1	0.348	0.550	18.1	37.4

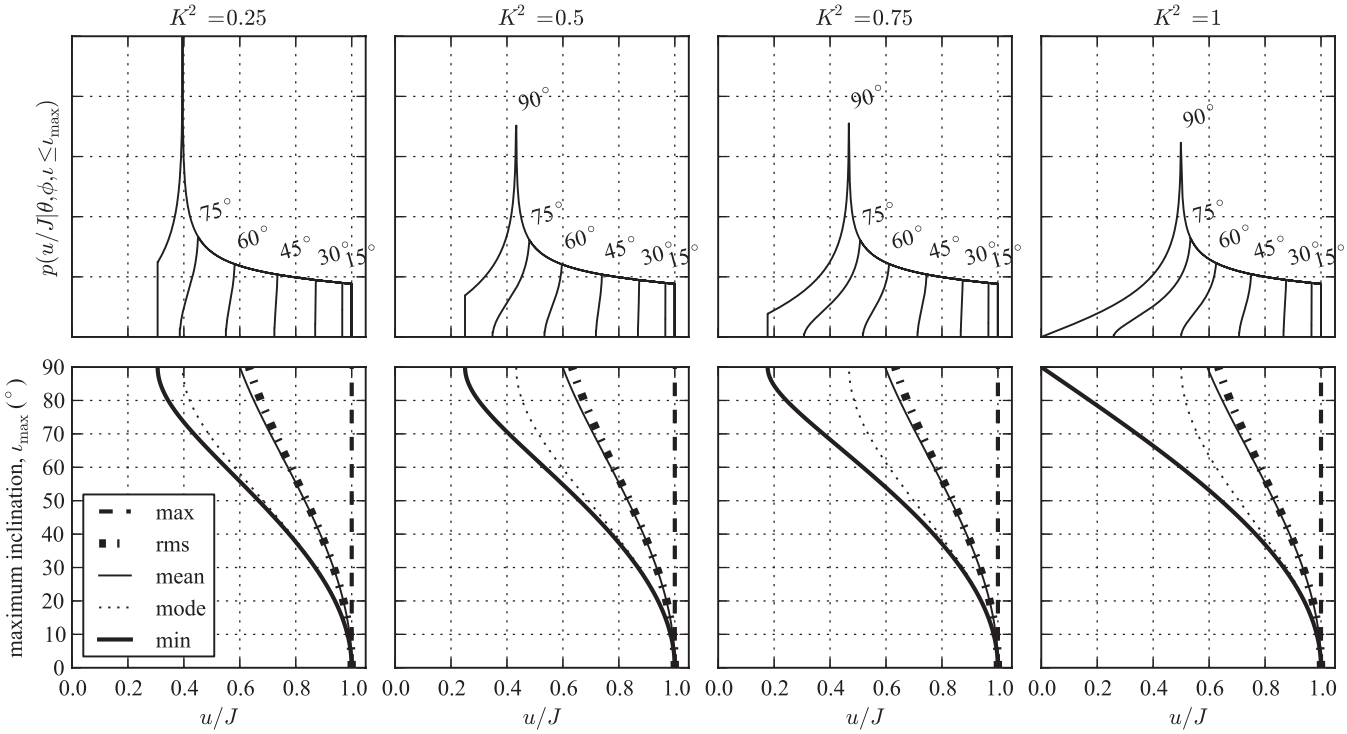

FIG. 3. Prior distribution of (u/J), the distance-independent part of the detector response, normalized by the detector's root-sum-squared antenna pattern at a given sky location. The top row shows the probability density function itself, for jet opening angles of 15° to 90°. From left to right, the value of K^2 is varied from 0.25 to 0.1, smoothly varying from a detector configuration that has similar sensitivity to two polarizations to a configuration that is sensitive to only one polarization. The bottom row of plots shows five summary statistics of the distribution: the minimum, maximum, mean, mode, and rms.

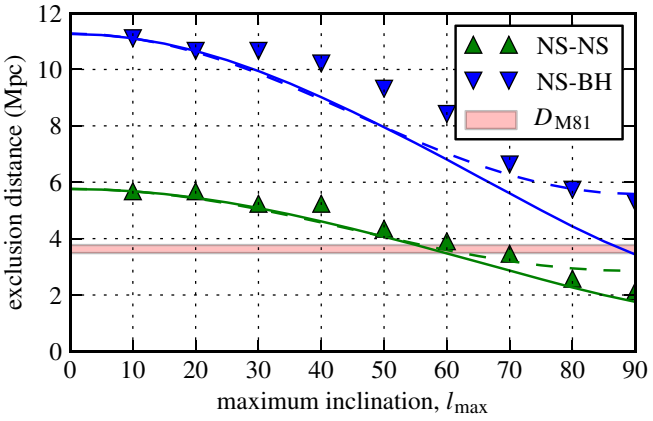

FIG. 4 (color online). Exclusion distance as a function of $\iota_{\rm max} = \theta_j$. The filled triangles are the 90%-confidence exclusion distances from Fig. 3 of Abadie *et al.* [20]. The up arrows (green in the online version) represent the NS-NS signal model, and the down arrows (blue in the online version) represent the NS-BH signal model. The solid curves show the 10% value of the inverse CDF of (u/J), scaled to match the exclusion distance at $\iota_{\rm max} = 10°$. The dashed curves show the mode of the distribution of (u/J), also scaled to match the exclusion distance at $\iota_{\rm max} = 10°$. The pink band marks the distance to M81, 3.63 ± 0.14 Mpc.

θ_j. Where θ_j is small, we approximate the GW amplitude for GRB-triggered sources to be on average ~1.51 times the isotropic detection-averaged amplitude for all CBCs, which is the instantaneous $\iota = 0$ value.

Using intermediate results from Appendix A, the azimuthally averaged detector response to a binary whose orbital plane is inclined at angle ι relative to the observer's line of sight is proportional to

$$\left(\frac{u}{J}\right)^2 = \frac{1}{8}(x^4 + 6x^2 + 1), \tag{B1}$$

where $x = \cos\iota$ and $J^2 = F_+^2 + F_\times^2$. The distance to which a GW source is detectable scales as u/J, so the number of detectable sources scales as $(u/J)^3$. Thus, the detection-averaged amplitude of all the sources that we observe within the half-angle θ_j is

$$\bar{A}(x_0) = \left[\int_{x_0}^{1}\left(\frac{u}{J}\right)^3 p(x)dx\right]^{1/3}, \tag{B2}$$

where $x_0 = \cos\theta_j$ and $p(x) = (1 - x_0)^{-1}$.

Using Eq. (B2), one easily shows that as long as the beam half-angle is $\lesssim 25°$, then average amplitude enhancement relative to an unrestricted distribution is at most a ~5% overestimate.

[1] C. Kouveliotou, C. A. Meegan, G. J. Fishman, N. P. Bhat, M. S. Briggs, T. M. Koshut, W. S. Paciesas, and G. N. Pendleton, Astrophys. J. **413**, L101 (1993).
[2] I. Horvath, Astron. Astrophys. **392**, 791 (2002).
[3] B. Abbott *et al.* (LIGO Scientific Collaboration), Astrophys. J. **681**, 1419 (2008).
[4] A. Dietz (LIGO Scientific Collaboration), AIP Conf. Proc. **1000**, 284 (2008).
[5] J. Abadie, B. P. Abbott, R. Abbott, T. Accadia, F. Acernese, R. Adhikari, P. Ajith, B. Allen, G. Allen, E. Amador Ceron *et al.*, Astrophys. J. **715**, 1453 (2010).
[6] H.-Y. Chen and D. E. Holz, arXiv:1206.0703.
[7] L. Z. Kelley, I. Mandel, and E. Ramirez-Ruiz, arXiv:1209.3027.
[8] S. Nissanke, M. Kasliwal, and A. Georgieva, arXiv:1210.6362 [Astrophys. J. (to be published)].
[9] C. Cutler and E. Flanagan, Phys. Rev. D **49**, 2658 (1994).
[10] L. S. Finn and D. F. Chernoff, Phys. Rev. D **47**, 2198 (1993).
[11] E. Poisson and C. M. Will, Phys. Rev. D **52**, 848 (1995).
[12] R. O'Shaughnessy, C. Kim, V. Kalogera, and K. Belczynski, Astrophys. J. **672**, 479 (2008).
[13] É. É. Flanagan and T. Hinderer, Phys. Rev. D **77**, 021502 (2008).
[14] J. S. Read, C. Markakis, M. Shibata, K. Uryū, J. D. E. Creighton, and J. L. Friedman, Phys. Rev. D **79**, 124033 (2009).
[15] C. M. Will, Living Rev. Relativity **9**, 3 (2006), http://www.livingreviews.org/lrr-2006-3.
[16] J. Ellis, N. Mavromatos, D. Nanopoulos, A. Sakharov, and E. Sarkisyan, Astropart. Phys. **25**, 402 (2006).
[17] A. Stavridis and C. M. Will, Phys. Rev. D **80**, 044002 (2009).
[18] D. Keppel and P. Ajith, Phys. Rev. D **82**, 122001 (2010).
[19] N. Dalal, D. E. Holz, S. A. Hughes, and B. Jain, Phys. Rev. D **74**, 063006 (2006).
[20] J. Abadie, B. P. Abbott, T. D. Abbott, R. Abbott, M. Abernathy, C. Adams, R. Adhikari, C. Affeldt, P. Ajith, B. Allen *et al.*, Astrophys. J. **755**, 2 (2012).
[21] J. Abadie, B. P. Abbott, R. Abbott, T. D. Abbott, M. Abernathy, T. Accadia, F. Acernese, C. Adams, R. Adhikari, C. Affeldt *et al.*, Astrophys. J. **760**, 12 (2012).
[22] V. Pal'Shin, GCN Circ. **6098**, 1 (2007).
[23] K. Hurley *et al.*, GCN Circ. **6103**, 1 (2007).
[24] K. Hurley, A. Rowlinson, E. Bellm, D. Perley, I. G. Mitrofanov, D. V. Golovin, A. S. Kozyrev, M. L. Litvak, A. B. Sanin, W. Boynton *et al.*, Mon. Not. R. Astron. Soc. **403**, 342 (2010).
[25] I. W. Harry and S. Fairhurst, Phys. Rev. D **83**, 084002 (2011).
[26] H. B. Mann and D. R. Whitney, Ann. Math. Stat. **18**, 50 (1947).
[27] B. Abbott *et al.* (LIGO Scientific Collaboration), Rep. Prog. Phys. **72**, 076901 (2009).
[28] F. Acernese *et al.*, Classical Quantum Gravity **25**, 184001 (2008).
[29] G. M. Harry (LIGO Scientific Collaboration), Classical Quantum Gravity **27**, 084006 (2010).
[30] H. Grote (LIGO Scientific Collaboration), Classical Quantum Gravity **27**, 084003 (2010).
[31] B. Willke, P. Ajith, B. Allen, P. Aufmuth, C. Aulbert, S. Babak, R. Balasubramanian, B. W. Barr, S. Berukoff, A. Bunkowski *et al.*, Classical Quantum Gravity **23**, S207 (2006).
[32] K. Kuroda, Classical Quantum Gravity **27**, 084004 (2010).
[33] T. Uchiyama *et al.*, Classical Quantum Gravity **21**, S1161 (2004).
[34] K. Hurley (private communication).
[35] D. N. Burrows (private communication).
[36] C. A. Wilson-Hodge, G. L. Case, M. L. Cherry, J. Rodi, A. Camero-Arranz, P. Jenke, V. Chaplin, E. Beklen, M. Finger, N. Bhat *et al.*, Astrophys. J. Suppl. Ser.**201**, 33 (2012).
[37] N. Gehrels, S. D. Barthelmy, and J. K. Cannizzo, Proc. Int. Astron. Union **7**, 41 (2012).
[38] J. Paul, J. Wei, S. Basa, and S.-N. Zhang, C.R. Physique **12**, 298 (2011).
[39] S. Basa (private communication).
[40] B. Grossan, I. H. Park, S. Ahmad, K. B. Ahn, P. Barrillon, S. Brandt, C. Budtz-Jørgensen, A. J. Castro-Tirado, P. Chen, H. S. Choi *et al.*, arXiv:1207.5759.
[41] S. D. Barthelmy *et al.*, Space Sci. Rev. **120**, 143 (2005).
[42] D. Grupe, D. N. Burrows, S. K. Patel, C. Kouveliotou, B. Zhang, P. Meszaros, R. A. M. Wijers, and N. Gehrels, Astrophys. J. **653**, 462 (2006).
[43] D. N. Burrows *et al.*, Astrophys. J. **653**, 468 (2006).
[44] A. Goldstein *et al.*, arXiv:1101.2458.
[45] W.-f. Fong, E. Berger, R. Margutti, B. A. Zauderer, E. Troja, I. Czekala, R. Chornock, N. Gehrels, T. Sakamoto, D. B. Fox *et al.*, arXiv:1204.5475.
[46] F. Foucart, M. D. Duez, L. E. Kidder, and S. A. Teukolsky, Phys. Rev. D **83**, 024005 (2011).
[47] J. Abadie, B. P. Abbott, R. Abbott, T. D. Abbott, M. Abernathy, T. Accadia, F. Acernese, C. Adams, R. Adhikari, C. Affeldt *et al.*, Phys. Rev. D **85**, 082002 (2012); data available online at https://dcc.ligo.org/LIGO-P1100034-v19/public.
[48] C. S. Kochanek and T. Piran, Astrophys. J. Lett.**417**, L17 (1993).
[49] B. F. Schutz, Classical Quantum Gravity **28**, 125023 (2011).
[50] M. Boyle, A. Buonanno, L. Kidder, A. Mroué, Y. Pan, H. Pfeiffer, and M. Scheel, Phys. Rev. D **78**, 104020 (2008).
[51] J. Abadie, B. P. Abbott, R. Abbott, M. Abernathy, T. Accadia, F. Acernese, C. Adams, R. Adhikari, P. Ajith, B. Allen *et al.*, Classical Quantum Gravity **27**, 173001 (2010).
[52] U. Takashi (private communication).
[53] LIGO, Advanced LIGO Anticipated Sensitivity Curves, https://dcc.ligo.org/T0900288-v3/public.
[54] Virgo, Advanced Virgo Sensitivity, https://wwwcascina.virgo.infn.it/advirgo/.
[55] KAGRA, KAGRA Parameters, http://gwcenter.icrr.u-tokyo.ac.jp/en/researcher/parameter.
[56] C. Messenger and J. Veitch, arXiv:1206.3461.